

3D mapping of the Wolf-Rayet nebula M 1-67: clues for post-common envelope evolution in massive stars

S. Zavala^{1*}, J.A. Toalá², E. Santamaría^{3,4}, G. Ramos-Larios^{3,4}, L. Sabin⁵, J.A. Quino-Mendoza^{3,4}, G. Rubio^{3,4} and M.A. Guerrero⁶

¹Tecnológico Nacional de México / I. T. Ensenada, Depto. de Ingeniería Eléctrica y Electrónica, C. P. 22780 Ensenada, B.C., Mexico

²Instituto de Radioastronomía y Astrofísica (IRyA), UNAM Campus Morelia, Apartado postal 3-72, 58090 Morelia, Michoacán, Mexico

³CUCEI, Universidad de Guadalajara, Blvd. Marcelino García Barragán 1421, 44430, Guadalajara, Jalisco, Mexico

⁴Instituto de Astronomía y Meteorología, Depto. de Física, CUCEI, Av. Vallarta 2602, 44130, Guadalajara, Jalisco, Mexico

⁵Instituto de Astronomía, Universidad Nacional Autónoma de México, Apdo. Postal 877, C.P. 22860, Ensenada, B.C., Mexico

⁶Instituto de Astrofísica de Andalucía, IAA-CSIC, Glorieta de la Astronomía s/n, 18008, Granada, Spain

19 April 2022

ABSTRACT

We present a 3D mapping of the Wolf-Rayet (WR) nebula M 1-67 around WR 124. We obtained high-resolution San Pedro Mártir (SPM) Manchester Echelle Spectrograph (MES) observations along 17 long-slit positions covering all morphological features in M 1-67. We are able to unveil the true morphology of M 1-67 and its kinematics by interpreting the SPM MES observations by means of the 3D modelling tool for Astrophysics SHAPE. Our SHAPE model that best reproduces the SPM MES data includes three concentric bipolar structures composed by a hollow ellipsoidal structure and a torus. In addition, the model requires the presence of expanding jets and broken blisters in order to reproduce specific spectral features. Our results are consistent with the idea that M 1-67 and its progenitor star WR 124 have formed through a common envelope scenario that occurred $11.8^{+4.6}_{-0.8}$ kyr ago. Our bipolar model strongly questions previous suggestions of the presence of a bow shock structure surrounding M 1-67. We interpret that the bright structures detected in the spectra extracted from the central regions are produced by wind compression at the receding region of the innermost structure in M 1-67. Furthermore, WR 124 is moving through a low-density region above the Galactic plane that has negligibly affected the formation history of M 1-67.

Key words: Massive stars — stars: evolution — stars: mass loss — stars: circumstellar matter — stars: individual (WR124)

1 INTRODUCTION

Wolf-Rayet (WR) nebulae form as the result of the historic mass loss from massive stars. It is accepted that single massive stars might lose most of their H-rich envelopes while evolving through a red supergiant (RSG) or luminous blue variable (LBV) phase (Conti 1975). In the case of binary systems, the ejection of the H-rich envelope can also be produced by the interaction with a companion through a common envelope phase (Paczynski 1967). Regardless of the process of mass ejection, the resultant star is a H-deficient, He-rich star that possesses powerful stellar winds ($v_\infty \gtrsim 1500$ km s⁻¹, $\dot{M} \approx 10^{-5} M_\odot$ yr⁻¹; Hamann et al. 2019) leading to strong emission lines of C, N and O (e.g., Crowther et al. 1998). The winds from WR stars sweep and compress the previously ejected material into ring-like structures, while the newly developed UV flux photoionizes it, creating a WR nebula (García-Segura & Mac Low 1995a,b).

Numerical simulations have demonstrated that such interaction create young ring nebulae that in time experience hydrodynamical instabilities that will subsequently disrupt the shell into clumps and filaments (e.g., García-Segura et al. 1996; Freyer et al. 2006; Toalá

& Arthur 2011). Observationally, WR nebulae exhibit a double shell morphology at optical wavelengths. Most of the emission is detected in H α +[N II] images tracing the bulk of the mass of the nebula with an external [O III] shell unveiling the leading shock into the interstellar medium (ISM; e.g., Gruendl et al. 2000).

Unlike other WR nebulae, the clumpy morphology of M 1-67 (Fig 1; e.g., Fernández-Martín et al. 2013, and references therein) seems to suggest a different origin than the wind-wind interaction scenario described above. Its progenitor star, the WN8h star WR 124, (a.k.a. Merrill’s star), is one of the fastest runaway WR stars in our Galaxy with a stellar radial velocity ~ 180 km s⁻¹ (see, e.g., Kharchenko et al. 2007). At an estimated distance of $6.4^{+2.5}_{-0.8}$ kpc (see Jiménez-Hernández et al. 2020), WR 124 is located ~ 370 pc above the Galactic Plane. Many studies have discussed the origin of this peculiar velocity and its location outside the Galactic plane. Either WR 124 interacted gravitationally with a group of massive stars (Crowther 2007) or it was pulled out of the galactic plane due to a supernova explosion of an undetected neutron star companion (Chu & Treffers 1981; Toalá et al. 2018).

The unprecedented view offered by the narrow-band images of the *Hubble Space Telescope* (HST) (see Fig. 1) suggests that M 1-67 is composed of ballistic expanding knots (Grosdidier et al. 1998;

* E-mail: szavala@ite.edu.mx

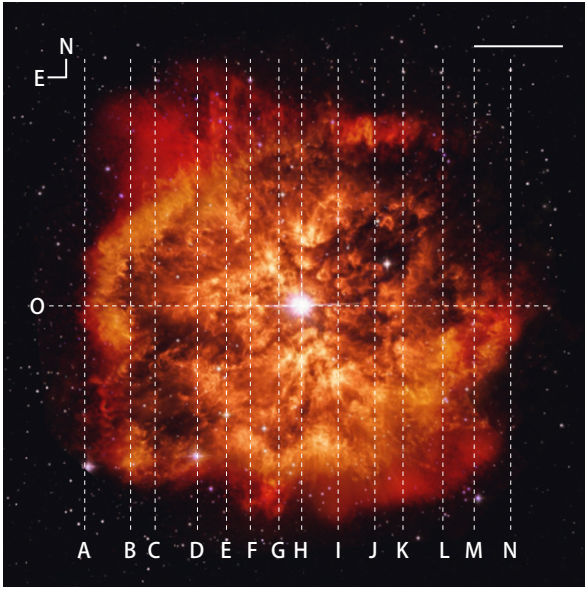


Figure 1. *HST* image of M1 67 around WR 124. The dotted lines represent the positions of the SPM-MES slits. Note that the H and O slits crosses the central star at PA=0° and PA=90° respectively. The horizontal white bar at the top right corner represents 20″.

Marchenko, Moffat & Crowther 2010) as well as clumps and filaments resulting from instabilities. The inspection of the *HST* images has shown that clumps expanding at position angles (PA) of $\sim 20^\circ$ and $\sim 200^\circ$ exhibit V-shaped morphologies, the so-called *Mach cones* (Grosdidier et al. 1998). The optical photometric and spectroscopic variability presented by WR 124 (Moffat et al. 1982) and the bipolarity exhibited by M 1-67, clearly unveiled by IR images (Gvaramadze et al. 2010) with broken structures located at PA ≈ 110 and -70° , support the idea of a possible binary system at the core of this WR nebula.

Jiménez-Hernández et al. (2020) used multi-mission IR observations in addition to publicly available optical observations of M 1-67 to simultaneously model its nebular and dust properties with the photoionization code CLOUDY. The population of dust sizes ($\lesssim 1\mu\text{m}$) and the amount of dust present in the nebula led Jiménez-Hernández et al. (2020) to suggest that the iconic M 1-67 nebula has been formed through an eruptive wind (e.g., Kochanek 2011). In particular, these authors propose that M 1-67 has been formed through a common envelope channel (see Podsiadlowski et al. 2010), a phase that produced M 1-67 by expelling the H-rich layers of its progenitor star in a bipolar fashion and also giving birth to WR 124.

Several works have addressed the kinematics of M 1-67 to try to unveil its true morphology and formation history. Solf & Carsenty (1982) used high-resolution optical spectra of this WR nebula and suggested that its velocity field could be explained by an almost spherical thin shell expanding at a velocity of 42 km s^{-1} . Similar results were also reported by Sirianni et al. (1998), who in addition to the spherical cavity, suggested the presence of a bipolar outflow with an expansion velocity of 88 km s^{-1} . It has also been argued that WR 124 would be able to form a bow shock structure given its high velocity with respect to the ISM (see, e.g., Meyer et al. 2020). This idea was initially explored by van der Sluys & Lamers (2003), who suggested that a bow shock is located at the region preceding M 1-67 so that we are seeing through it, along the main axis.

Recently, Sévigny et al. (2021) presented imaging Fourier trans-

Table 1. Details of the SPM-MES observations of M 1-67. The offsets are denoted with respect to the position of the central star WR 124.

Slits	Offset (″)	Filter	PA (°)	Date	Exp. Time (s)
A	-53.6	H α + [N II]	0	2018 May 6	600
B	-41.1	H α + [N II]	0	2018 May 6	600
C	-34.4	H α + [N II]	0	2018 May 6	600
D	-26.8	H α + [N II]	0	2018 May 6	600
E	-18.0	H α + [N II]	0	2018 May 6	600
F	-11.3	H α + [N II]	0	2018 May 6	600
G	-5.1	H α + [N II]	0	2018 May 6	600
H	0.0	H α + [N II]	0	2018 May 6	600
H	0.0	[S II]	0	2019 May 27	600
H	0.0	[O III]	0	2019 May 27	1800
I	9.4	H α + [N II]	0	2018 July 22	600
J	16.5	H α + [N II]	0	2018 July 22	600
K	23.8	H α + [N II]	0	2018 July 22	600
L	32.1	H α + [N II]	0	2018 July 22	600
M	41.1	H α + [N II]	0	2018 July 22	600
N	49.6	H α + [N II]	0	2018 July 22	600
O	0.0	[S II]	90	2018 July 22	600

form spectrometer SITELE observations obtained at the Canada-France-Hawaii Telescope (CFHT). These authors presented several emission line maps centered on the H α , [N II] 6584 Å, [N II] 5755 Å, [S II] 6717+6731 Å, He II 4686 Å, including an unprecedented [O II] image of M 1-67¹. Their observations confirm the bipolar structure of M 1-67 with its axis positioned at PA $\approx -70^\circ$. These authors used the relatively low spectral resolution of the SITELE observations to suggest that the kinematical structures in M 1-67 are consistent with that of the bow shock suggested by previous works.

In this work, we present a comprehensive morpho-kinematic model of M 1-67 using a set of high resolution spectra that cover most of this WR nebula. Our data are interpreted by means of the interactive 3D SHAPE software (Steffen et al. 2011; Koning & Steffen 2012), that helped us reconstruct the morphology and kinematic structure of M 1-67 to revise its formation history based on their dynamical processes. This paper is organized as follows. The observations are described in Section 2 and the kinematic results are presented in Section 3. A morpho-kinematic model of M 1-67 is described in Section 4. Finally, our discussion and summary are presented in Sections 5 and 6, respectively.

2 OBSERVATIONS

Long-slit, high resolution spectroscopic observations were obtained using the Manchester Echelle Spectrometer (MES; Meaburn, et al. 2003) mounted on the 2.1 m telescope at the Observatorio Astronómico Nacional in San Pedro Mártir (SPM, Ensenada, Mexico). The observations of M 1-67 were conducted in several runs, initiating on 2018 May 6 and July 22 and concluding on 2019 May 27. We used the 2k \times 2k CCD with a pixel scale of $13.5\mu\text{m pix}^{-1}$ and 2 \times 2 on-chip binning which resulted in a plate scale of $0.351\text{ arcsec pix}^{-1}$. A summary of the observations is presented in Table 1.

A total of 15 slit positions were used to obtain 17 high-resolution SPM MES spectra of M 1-67. The positions of the slits are shown in

¹ We note that although Sévigny et al. (2021) reported the presence of the [O III] emission line in their table 3, they did not present its corresponding line map.

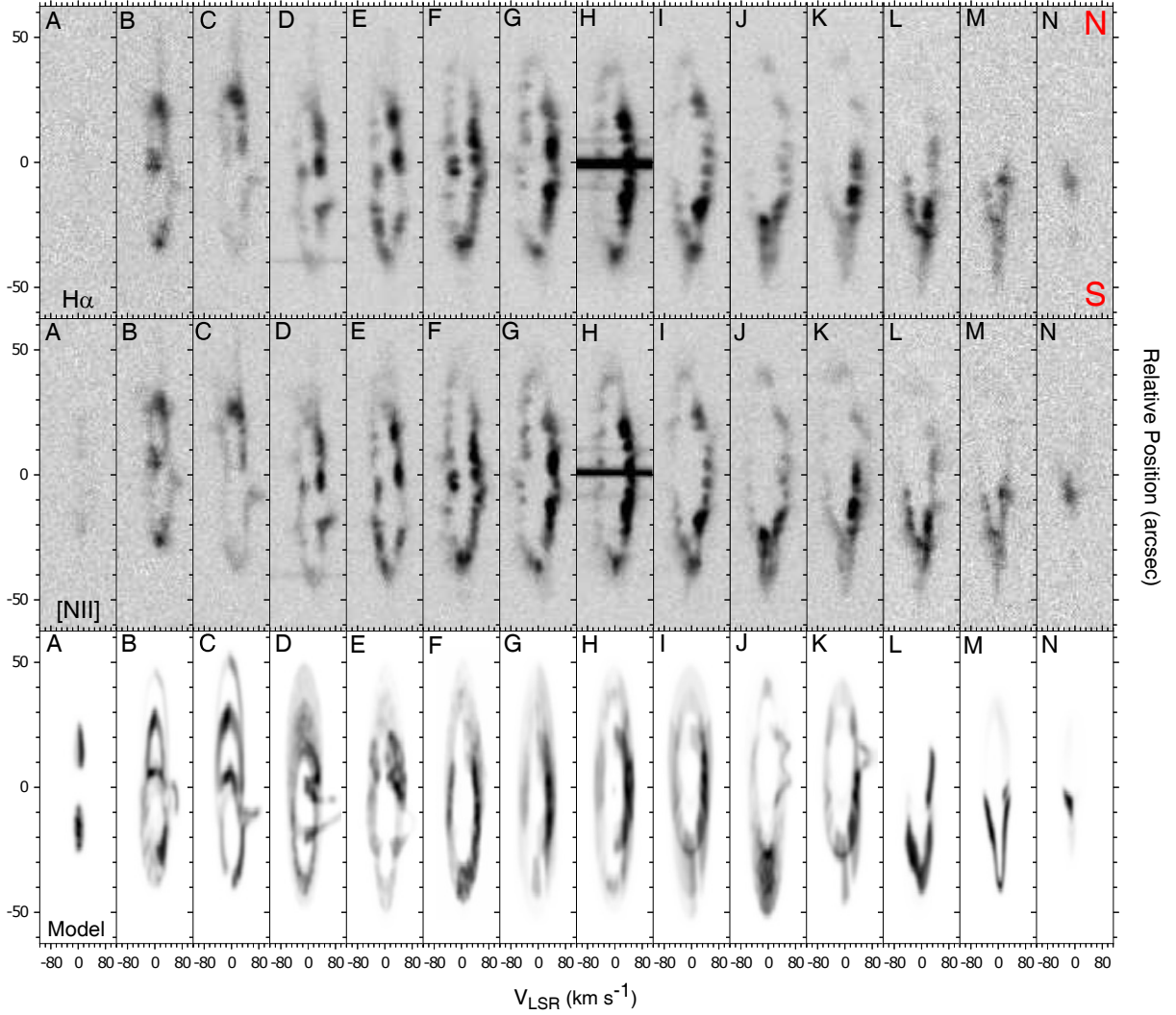


Figure 2. Position Velocity (PV) diagrams of the H α (top) and [N II] 6584 Å (middle) spectra obtained from our SPM-MES observations. The bottom row presents the synthetic PV diagrams obtained from our best SHAPE model (see Sec. 4). The N-S direction is labelled in the top right panel. The horizontal line visible on the H spectra is produced by the central star which has a relative position of 0

Figure 1. We obtained 14 spectra with a position angle (PA) of 0° labeled from A to N using the $\lambda_c=6580$ and $\Delta\lambda=90$ Å interference filter which isolates the 87th order and includes the wavelength region encompassing the emission lines of [N II] 6548 Å, He II 6560 Å, H α , C II 6578 Å and [N II] 6584 Å. Additionally, two spectra at PA=0° and 90° at the H and O positions, respectively, were obtained using the interference filter $\lambda_c=6730$ Å and $\Delta\lambda=90$ Å that include the emission of the [S II] $\lambda\lambda 6717, 6731$ Å doublet. All observations were obtained with exposure times of 600 s and a slit width of 150 μm (~ 2 arcsec) that result in a velocity resolution of 12 km s⁻¹.

Finally, one slit position at PA of 0° was acquired with the interference filter $\lambda_c=5020$ Å and $\Delta\lambda=70$ Å that includes the emission line of [O III] $\lambda 5007$ Å. This spectrum has an exposure time of 1800 s. Most spectra were obtained with a chip binning of 2 \times 2, except for the O position which was obtained with a 4 \times 4 binning.

All SPM-MES spectra were reduced using standard calibration routines in IRAF (Tody 1993), including bias subtraction and wavelength calibration with a Th/Ar arc lamp for an accuracy of ± 1 km s⁻¹.

3 RESULTS

The SPM-MES H α and [N II] 6584 Å spectra of M 1-67 are presented in the top and middle rows of Figure 2. We also detected the [N II] 6548 Å, but due to its intrinsically lower surface brightness we do not show it here. We do not detect the He II 6560 Å nor the C II 6578 Å line in the spectra. Finally, we note that we do not detect neither any hint of [O III] emission in the spectrum taken at slit H (not shown here).

The spectra shown in Figure 2 resemble those presented by previous works (see Section 1). Spectra taken from the central regions of M 1-67 exhibit a cavity that departs from a shell-like morphology. For example, the receding parts of the G, H and I PV diagrams are brighter than the approaching structure (see also Solf & Carsenty 1982). Using Gaussian fits to the spectra obtained through slit H we determined the systemic velocity (V_{sys}) of WR 124. These resulted in 170.5 ± 10 km s⁻¹ for H α , 169.5 ± 8 km s⁻¹ for [N II] and 178 ± 5 km s⁻¹ for [S II].

Using Slit H to assess an averaged expansion velocity of the central

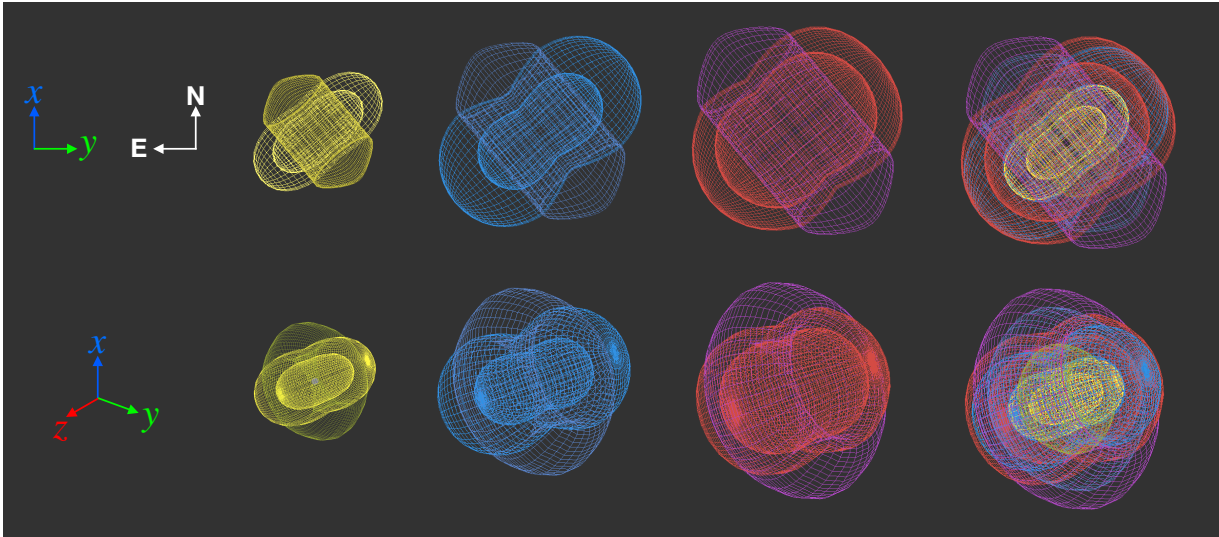


Figure 3. Different structures used in our basic *SHAPE* model of M 1-67. The inner, intermediate and outer structures are shown with different colours. The top row shows the structures in the plane of the sky, whilst the bottom row shows a randomly-selected viewing angle for further illustration. The colour arrows show the *SHAPE* coordinate system. The right-most figures show the combination of the different structures.

Table 2. Morphology and velocity parameters of the three main structures in our *SHAPE* model (see Fig. 4).

Parameter	Inner Structure	Middle Structure	Outer Structure
Hollow ellipsoidal component			
a_{out} ["]	35.0	55.0	55.0
a_{inn} ["]	25.0	43.0	46.0
b_{out} ["]	15.8	24.2	35.8
b_{inn} ["]	11.3	18.9	29.9
η	0.55	0.56	0.35
$v(r)$ [km s ⁻¹]	90($r/35$)	90($r/55$)	90($r/55$)
Toroidal component			
r_{out} ["]	30.0	50.0	60.0
r_{inn} ["]	13.8	25.0	30.0
l ["]	14.0	25.0	30.0
$v(r)$ [km s ⁻¹]	60($r/30$)	60($r/50$)	60($r/60$)

inner cavity of M 1-67 we obtained 46.3 ± 3.0 km s⁻¹, very similar to values reported in previous works (see for example [Solf & Carsenty 1982](#); [Sirianni et al. 1998](#)). Averaging the velocities of the inner hollow region from slits F to J we obtained 44 ± 13 km s⁻¹. This procedure is more difficult to apply to spectra taken at the eastern and western edges of M 1-67 because they disclose more complex structures than those of expanding shell-like structures. For example, the spectra taken with slits B seem to present a double lace morphology, whilst spectra obtained at positions C and D show a break out at relative position between 10 and 20 arcsec (see Fig. 2). Furthermore, the spectra show that the NW region of M 1-67 is fainter than the other regions, consistent with the emission line maps presented in previous works (see [Sévigny et al. 2021](#), and references therein).

The [S II] spectra also exhibit the uneven shell-like structure similarly to the H α profiles with the more intense part being the receding nebular regions, but with lower signal-to-noise. The expansion velocity estimated from these spectra is 46 ± 3 km s⁻¹, consistent with that obtained from other emission lines. Given that we detected the two [S II] 6717 Å and 6731 Å emission lines from each spectrum,

we tried to calculate electron density n_e maps, but their low signal-to-noise prevent us from discussing them further.

4 MORPHO-KINEMATIC MODEL

Taking advantage that the high-resolution SPM MES spectra presented here cover all the morphological features in M 1-67, we can disentangle its true morpho-kinematic structure using the modelling tool *SHAPE*. This software allows to construct 3D model structures and study the morphology of an astronomical object.

SHAPE can be used to define simple geometric shapes such as spheres, tori, cones or cubes in addition to expansion velocity patterns. Synthetic PV diagrams can be extracted from these structures to be compared with observations. If the synthetic spectra and images do not reproduce the observations, these shapes can be manually modified according to features that may be needed, for instance rotating these structures or stretching certain regions. This is an iterative process and a structure (or model) can be argued to be adequate if it reproduces a variety of observed morphological and spectral features. We note that *SHAPE* does not model physical density unless the hydrodynamical module is used, which is not the case here. Instead, the point density parameters are used to enhance the brightness in the user-defined kinematic structures. That is, the present *SHAPE* model can be only use to assess the kinematic structures in M 1-67.

We started our *SHAPE* modelling by defining a hollow spherical structure. The evident departure from spherical symmetry confirmed by the SPM MES observations forced us to add other structures with increased complexity. As a first approximation, we found that a basic model that reproduces the general kinematic features in the PV diagrams is that of a bipolar structure. In particular, the model requires three concentric structures, each composed by a torus and a bipolar structure to fit most of the spectral features of the line profiles. Each bipolar lobe is modelled by a hollow ellipsoidal component squished at the waist. These elements are illustrated in the top row of Figure 3. The three bipolar structures are contained within the plane of the sky and their symmetry axis are tilted with a PA = -40°. To illustrate them further, the bottom row shows a arbitrary viewing

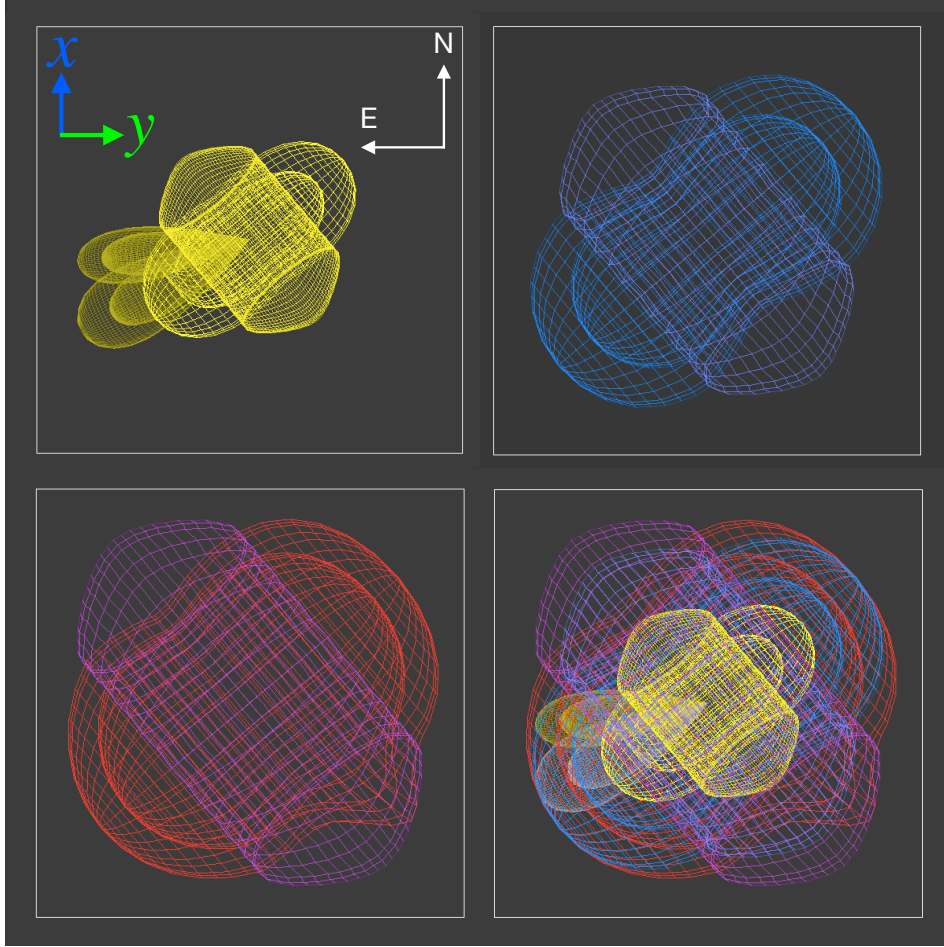


Figure 4. The best SHAPE model that reproduces the SPM MES observations. Different contributing structures are presented as well as a combination of all elements in the bottom right panel. The structures are shown as they would appear in the plane of the sky, which is defined by the $x - y$ ($z = 0$) plane in SHAPE.

angle of the model. The right-most panels in Figure 3 show the combination of the three kinematic components.

Each of the inner, middle and outer structures required different sizes and velocity patterns. Each of these is defined by a combination of parameters. The hollow ellipsoidal component is defined by a semi-major axis (a_{out}), inner semi-major axis (a_{inn}), the semi-minor axis (b_{out}), inner semi-minor axis (b_{inn}), a squish parameter (η). On the other hand, the tori components are defined by an inner and outer radius (r_{inn} and r_{out}) and a thickness (h). In Table 2 we list the values required for the three main structures.

Given the evident presence of ballistically-expanding clumps in M 1-67, we decided to use velocity functions that have a linear increase with distance r as

$$v(r) = A \left(\frac{r}{B} \right), \quad (1)$$

where A and B are constants, where B is defined by the largest feature of each structure component. For example, for the hollow ellipsoidal component is a_{out} and r_{out} for the toroidal components. The velocity function for each component are also listed in Table 2.

Although the combination of these three relatively simple bipolar structures is enough to model the general morpho-kinematic properties of M 1-67, these do not give a good description of the details unveiled by the MES PV diagrams. For example, those PV obtained from slits a few arcsecs towards the east or west from the central star,

e.g., the PVs extracted from slit B, C and D. To achieve such level of detail, we had to include additional features to the SHAPE model. These include fast expanding structures and deformations. The final view of our best SHAPE model of M 1-67 is presented in Figure 4. This figure shows the three main structures as they would appear in the plane of the sky, which is defined by the $x - y$ ($z = 0$) plane in our SHAPE model.

Figure 4 shows that there is no need to modify the middle structure, but the outer one had to be deformed towards the SW direction. However, the inner structure requires noticeable modifications. We included a couple of fast expanding collimated structures which apparently protrude towards the SE. For simplicity, we will refer to these features as Jet 1 and Jet 2. Jet 1 was modelled with an apparent PAs of 120° in the plane of the sky while Jet 2 was placed at an apparent PA= 129° . Nevertheless, these structures are not contained in the plane of the sky ($z = y$, $z = 0$), but are expanding away from us with angles of 15° and 55° with respect to the plane of the sky. This situation is illustrated further in the left and middle panels of Figure 5. Their velocities are needed to be $v(r) = 90(r/75)$ and $90(r/56)$ for Jet 1 and 2, respectively, where $75''$ and $56''$ represent their total angular extension.

Additional blowouts are needed to model some of the specific features in the PV diagrams. These are just represented by two conical features on top of the hollow ellipsoidal component (see Fig. 5 middle

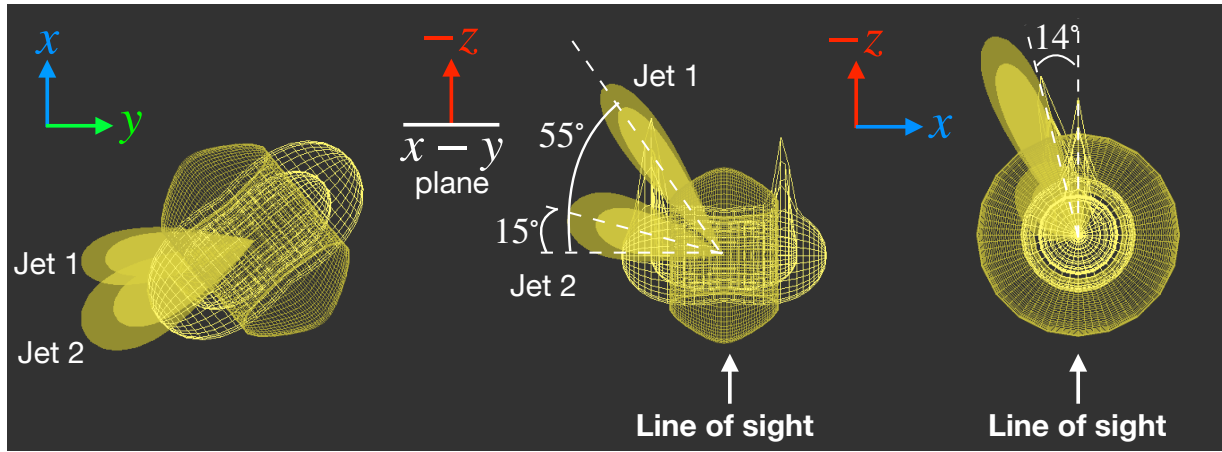


Figure 5. Different views of the inner structure of our best SHAPE model. The left figure shows the inner structure in the plane of the sky (see left top panel in Fig. 4). The middle and right panels are just rotations of the figure presented in the left.

panel). These are also needed towards the receding region of the structure, with one of them completely contain within the line of sight and the other one 14° towards the S direction (see the right panel of Fig. 5).

4.1 Comparison with observations

In Figure 6 we present a rendered synthetic image of our best SHAPE model combining all the structures described in the previous section. We have added Perlin noise to the different structures to produce an apparent clumpy morphology. In addition, we modified the density of points of the SHAPE model to mimic the variations of the surface brightness of the optical images of M 1-67. This effect is most evident in the NW region where there is no apparent emission from M 1-67 and the PV diagrams show almost negligible contribution. The extraction position of the synthetic PV diagrams is also overplotted on the synthetic image of Figure 6. Synthetic spectra were extracted from these positions and their resulting synthetic PV diagrams are plotted in the bottom row of Figure 2 for comparison with the observed PV obtained from the $H\alpha$ and $[\text{N II}]\lambda 6584 \text{ \AA}$ spectra.

The comparison between the observed and synthetic PVs presented in Figure 2 demonstrates that our SHAPE model successfully reproduces all observed spectral features. The central PVs, those obtained from slits G, H and I, are reproduced by reducing the density of points of the preceding side of the inner structure. This creates brighter spectra in the inner region of the PV diagrams towards red shifted velocities. This results in the bow shock-like apparent structure described in previous works (see Section 1). The reduction of the density of points towards the NW of the synthetic image also helps modelling the L, M and N PV diagrams.

To illustrate further the contribution from the three different kinematic structures in our SHAPE model we show in Figure 7 details of the synthetic spectra obtained from slits B and H. The contribution from the inner structure to slit B, shown in yellow, is mainly due to the presence of Jets 1 and 2. On the other hand, the contribution from the middle and outer structures are shown in blue and red in the PV diagrams. These produce double-lace features which are produced by the combination of the hollow-elliptical structures and the torii. A similar, decomposition of the spectrum H is also presented in the bottom row of Figure 7.

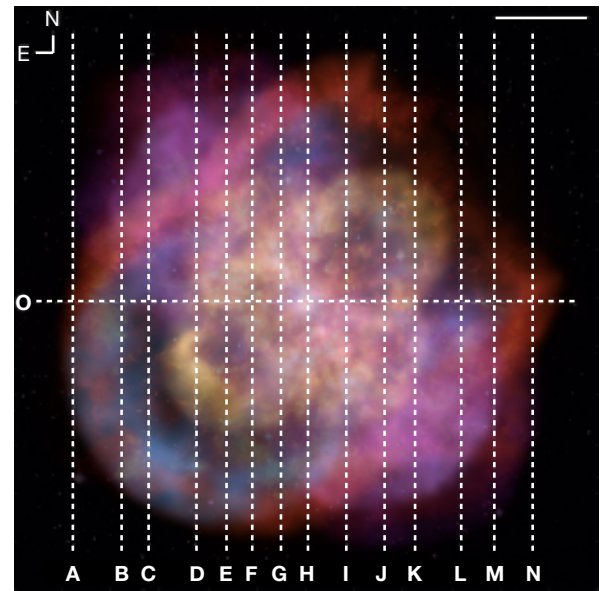


Figure 6. Synthetic image obtained by combining the three structures presented in Figure 3 and adding structure to our SHAPE model. The positions of the synthetic slits are illustrated with white dashed lines similarly to those in Figure 1. The horizontal white bar at the top right corner represents $20''$.

5 DISCUSSION

Jiménez-Hernández et al. (2020) used CLOUDY to model the nebular and dust grains properties of M 1-67. They concluded that dust with sizes as large as $0.9 \mu\text{m}$ are present in this WR nebula. Following Kochanek (2011) such large grains can only form around massive stars if their mass ejection has an eruptive nature with a mass-loss rate $> 10^{-3} M_\odot \text{ yr}^{-1}$. This would create dense structures with high opacities allowing the dust to grow. Jiménez-Hernández et al. (2020) estimated an initial mass for WR 124 of $\sim 40 M_\odot$ which according to stellar evolution models would not reach the LBV phase. Thus, they proposed a common envelope channel as an alternative formation scenario for the M 1-67+WR 124 system, which simultaneously helps explaining the eruptive nature suggested by their photoionisation model and the formation of the progenitor WR star. These results

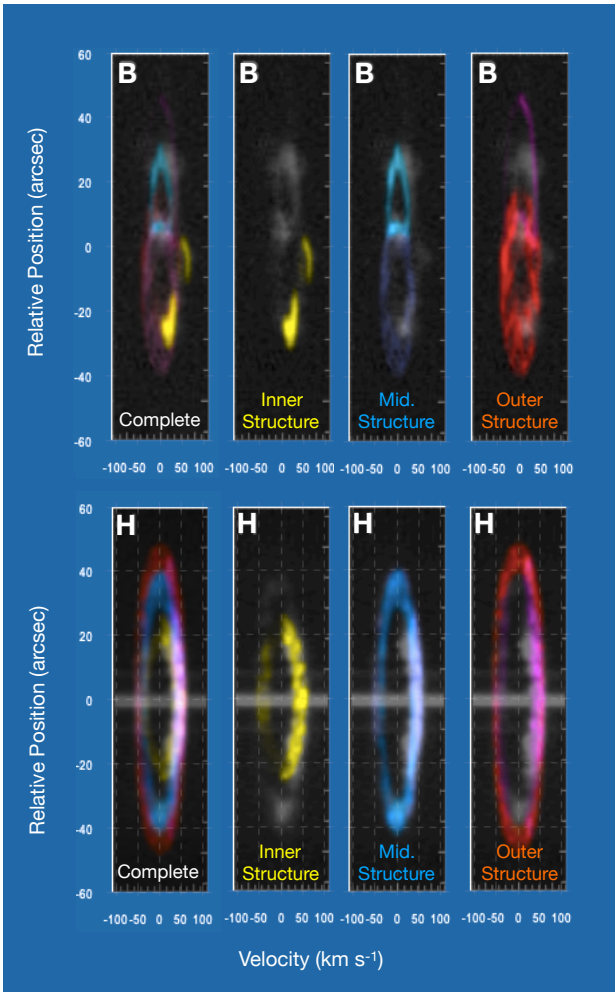


Figure 7. Contribution of the different kinematic components in our SHAPE model for slits B and H. The left most panel shows a combination from the three model components. The other panels show in yellow, blue and red the contributions from the inner, middle and outer structures in the SHAPE model.

might render M 1-67 as the first observational evidence for such an evolutionary channel of formation of a WR nebula.

The different kinematic structures needed to reproduce the SPM MES observations of M 1-67 seem to support the common envelope scenario proposed by Jiménez-Hernández et al. (2020). In general, our SHAPE model that best reproduces the observations is that of a bipolar nebula with the symmetry axis aligned with a PA = -40° . The main features in our SHAPE model are bipolar with toroidal components seen edge-on. The model requires the presence of three torii with similar velocity profiles with values ranging between ~ 30 and 60 km s^{-1} (see Table 2). We note however, that it is very likely that there is only a single toroidal structure surrounding M 1-67, a structure that has velocity variations or turbulence. The formation of toroidal structures via common envelope interactions are illustrated by different numerical simulations (Schröder et al. 2020) and predict that the density distribution during and after the common envelope evolution piles up material at the equatorial plane of the binary producing turbulent motions (see fig. 6 in Chamandy et al. 2019). Besides, the lower density of material in the polar regions naturally explains the formation of faster bipolar structures expanding perpendicularly from the orbital plane (e.g., Zou et al. 2020).

The later helps explaining the faster velocity patterns needed in our morpho-kinematic model of M 1-67 for the hollow elliptical structures. Their velocities range between ~ 30 and 90 km s^{-1} , evidently larger than those needed for the torii. The later is consistent with the detection of a bipolar outflow expanding at 88 km s^{-1} reported by Sirianni et al. (1998).

An explosive ejection mechanism of the common envelope as that presented and discussed in Podsiadlowski et al. (2010) would help explaining the Mach cones seen in the HST image of M 1-67, the presence of Jet 1 and 2 as well as the blowouts required at the receding part of the inner structure of our SHAPE model. These blowouts are reminiscent of possible fast ejections that disrupted and left the main structure of M 1-67. We note that no clear presence of jets/fast expanding features are detected in the preceding regions of the spectra and might be attributed to the low signal-to-noise of the blue shifted material. Although some deformation of the blue shifted material can be hinted in the PVs from the central regions of M 1-67 (see Fig. 2).

We conjecture that after the ejection of the H-rich envelope, the central WR star was born (see Paczyński 1967) developing a fast wind ($\sim 710 \text{ km s}^{-1}$ for WR 124; Hamann et al. 2019) that subsequently swept the bipolar structure creating a hollow inner structure. These interactions further facilitated the expansion of the material towards the polar regions enhancing the bipolar structure better seen in mid-IR images of this WR nebula (see Gvaramadze et al. 2010; Toalá et al. 2018). By definition, M 1-67 became a WR nebula when the fast wind from WR 124 started sweeping and compressing the previously ejected material forming the inner structure. Thus, we can use the properties of the inner structure in our best SHAPE model to estimate a dynamical age. This resulted in $11.8^{+4.6}_{-1.5} \text{ kyr}$, adopting a distance of $6.4^{+2.5}_{-0.8} \text{ kpc}$ (see Sec. 1).

Previous works have suggested that M 1-67 formed under the wind-wind interaction scenario described in Section 1. For example, Meyer et al. (2020) presented 3D numerical simulations of the formation of WR nebulae around runaway massive stars (see also Brighenti & D’Ercole 1995a,b) taking into account the time-evolution of the stellar wind parameters. We note that, under the wind-wind scenario Rayleigh-Taylor instabilities develop, but these are not dominant in M 1-67. Furthermore, the scenario presented by Meyer et al. (2020) would suggest that most of the mass of M 1-67 would be dominated by ISM, which is not the case (see Jiménez-Hernández et al. 2020, and references therein). On the other hand, the presence of Mach cones in M 1-67 suggests a ballistically-expanding shell formed as the result of an explosive event.

Recently, Jiménez-Hernández et al. (2021) showed that the WR nebula RCW 58 around the WN8h star WR 40 has similar nebular and dust size properties as those as M 1-67 and proposed a similar formation mechanism as that for M 1-67. These authors proposed that RCW 58 has an apparent ring-like morphology reminiscent of a toroidal structure that has been swept by the current fast wind from WR 40, which is oriented almost in the plane of the sky. On the other hand, the wind-wind interaction scenario might be accurate when explaining the morphology of the WR nebula around the WN8h star WR 16 (see Cichowolski et al. 2020).

Our SHAPE model of M 1-67 successfully reproduces the morphology and all the spectral features detected with the SPM MES observations. The SPM MES observations presented here cover all morphological features of M 1-67. Our best SHAPE model does not require the presence of a bow shock feature in order to reproduce the observed line profiles. Some authors have proposed a different interpretation for the observed PV diagrams obtained from M 1-67,

in particular those obtained at the central regions. It has been proposed that these are more consistent with the presence of a bow shock structure located at the receding side of this WR nebula (see [van der Sluys & Lamers 2003](#)). Recently, [Sévigny et al. \(2021\)](#) used CFHT SITELLE observations with moderate spectral resolution ($R = 1300$) and argue that their observations are also consistent with such a morphological component. The bipolar model presented here strongly questions the existence of a bow shock structure. In fact, the analytical bow shock model used in [Sévigny et al. \(2021\)](#), and originally presented in [van der Sluys & Lamers \(2003\)](#), can not fit a considerable amount of material with higher radial velocities than that of the proposed bow shock structure.

In order to reproduce the spectral signatures detected in slits G, H and I, we only required the density of points at the receding region of the inner structure of our SHAPE model to be larger than its preceding side, that is, that the region ahead of WR 124 is brighter. The PV diagrams obtained from the SPM MES observations show that the brightest region attributed to the presence of a bow shock is contained within the largest structure of M 1-67. Evidently, this can be easily explained by the fact that WR 124 is moving away from us, naturally compressing the preceding inner region of M 1-67 with its fast wind. We would like to remark that this is not a bow shock by strict definition (see [Henney & Arthur 2019](#), and references therein). A similar situation as that proposed here has been described in the illustration of figure 6 of [Solf & Carsenty \(1982\)](#). We suspect that M 1-67 and its runaway progenitor star WR 124 are too far from the Galactic plane that no substantial density from the ISM could help form a bow shock structure.

Thanks to the high spectral resolution allowed by SPM MES ($R \leq 100,000$), the full coverage of M 1-67 in addition to the interpretation using the 3D SHAPE software, we are able to unveil the true morpho-kinematics of this complex and iconic nebula. This therefore allowed a better and more accurate representation of the velocity and morphological structures found in the nebula. Our model is consistent with the idea that WR 124 is located at high altitude over the Galactic Plane where the density of the ISM is negligible and has not affect the morphology of M 1-67. Our model agrees with the proposed scenario that M 1-67 was formed as a result of an explosive common envelope phase of WR 124 with an unseen companion.

6 SUMMARY

We presented the analysis of high-resolution SPM MES spectra that cover all morphological features of the WR nebula M 1-67 around WR 124. The SPM-MES data are interpreted using the morpho-kinematic software SHAPE. We found that M 1-67 has in fact a bipolar structure with its symmetry axis oriented with a $PA = -40^\circ$. Our best SHAPE model includes three enclosed bipolar structures, each of them composed by a hollow ellipsoid surrounded by a torus. The toroidal structure expands with velocities in the 30 to 60 km s⁻¹ range, while the bipolar structure has maximum velocities of 90 km s⁻¹. In addition, the model requires the presence of jet-like features and blowouts piercing the different structures in order to reproduce some specific features unveiled by the observed PV diagrams.

Our morpho-kinematic SHAPE model of M 1-67 reinforces the idea that this WR nebula and its progenitor star WR 124 formed through an explosive common envelope scenario (see [Jiménez-Hernández et al. 2020](#)). This process initially produced a dust-rich structure with a toroidal distribution of material that should be aligned with the orbital plane of the binary progenitor system. At some point, the central binary system experienced an explosive event ejecting ballistically-

expanding material that pierced through the toroidal structure with some blister-like structures. Finally, after forming the central WR star, its current fast wind swept the structure carving an inner cavity. Our model predicts a kinematic age for M 1-67 of $11.8^{+4.6}_{-0.8}$ kyr.

Our morpho-kinematic model does not require the presence of a bow shock structure as suggested by previous authors. Instead, we suggest that the proper motion of WR 124 is compressing the receding region of the inner structure in M 1-67 producing the bright, arc-like features observed in the spectra extracted from the central regions of this WR nebula. We suggest that WR 124 has evolved in a low density region of the Galactic Plane that has not affected its formation. Our model represents an improved version of that initially proposed almost forty years ago by [Solf & Carsenty \(1982\)](#).

ACKNOWLEDGMENTS

The authors are grateful to the anonymous referee for comments and suggestions that improved the presentation of the model and its interpretation. SZ acknowledges support from (TecNM) 11189.21-P, from F. Ramos-DIEE/MIA/ITE, and M.E. González-DCB/ITE. JAT acknowledges funding from the Marcos Moshinsky Foundation (Mexico) and Dirección General de Asuntos del Personal Académico (DGAPA), Universidad Nacional Autónoma de México, through grants Programa de Apoyo a Proyectos de Investigación e Innovación Tecnológica (PAPIIT) IA101622. ES, JAQM and GR acknowledge support from Universidad de Guadalajara and Consejo Nacional de Ciencia y Tecnología (CONACyT) for a student scholarship. GR-L acknowledges support from CONACyT grant 263373 and Programa para el Desarrollo Profesional Docente (PRODEP, Mexico). LS acknowledges support from UNAM PAPIIT grant IN101819. MAG acknowledges support of grant PGC 2018-102184-B-I00 of the Ministerio de Educación, Innovación y Universidades cofunded with FEDER funds. This paper is based in part on ground-based observations from the Observatorio Astronómico Nacional at the Sierra de San Pedro Mártir (OAN-SPM), which is a national facility operated by the Instituto de Astronomía of the Universidad Nacional Autónoma de México. The authors thank the telescope operator P.F. Guillén for valuable guidance during several observing runs, and to the OAN-SPM staff for their valuable support. This work has made extensive use of the NASA's Astrophysics Data System.

DATA AVAILABILITY

The data underlying this article will be shared on reasonable request to the corresponding author.

REFERENCES

- Bailer-Jones C. A. L., Rybizki J., Fouesneau M., Mantelet G., Andrae R., 2018, *AJ*, 156, 58
- Brighenti, F. & D'Ercole, A. 1995, *MNRAS*, 273, 443
- Brighenti, F. & D'Ercole, A. 1995b, *MNRAS*, 277, 53
- Chamandy, L., Blackman, E. G., Frank, A., et al. 2019, *MNRAS*, 490, 3727
- Chu, Y.-H., & Treffers, R. R. 1981, *ApJ*, 249, 586
- Chu Y.-H., 1983, *Astrophys. J.* 269,202
- Cichowski, S., Duronea, N. U., Suad, L. A., et al. 2020, *MNRAS*, 495, 417
- Conti, P. S. 1975, *Memoires of the Societe Royale des Sciences de Liege*, 9, 193
- Crowther P. A., 2007, *ARA & A*, 45, 177
- Crowther, P. A., De Marco, O., & Barlow, M. J. 1998, *MNRAS*, 296, 367

- Fernández-Martín, A., Vílchez, J. M., Pérez-Montero, E., et al. 2013, *A&A*, 554, A104
- Freyer, T., Hensler, G., & Yorke, H. W. 2006, *ApJ*, 638, 262
- Gaia Collaboration, Brown, A. G. A., Vallenari, A., et al. 2018, *A&A*, 616, A1
- García-Segura, G. & Mac Low, M.-M. 1995, *ApJ*, 455, 145
- García-Segura, G. & Mac Low, M.-M. 1995, *ApJ*, 455, 160
- García-Segura, G., Mac Low, M.-M., & Langer, N. 1996, *A&A*, 305, 229
- Grosdidier, Y., Moffat, A. F. J., Joncas, G., & Acker, A. 1998, *ApJ*, 506, L127
- Gruendl, R. A., Chu, Y.-H., Dunne, B. C., et al. 2000, *AJ*, 120, 2670
- Gvaramadze, V. V., Kniazev, A. Y., & Fabrika, S. 2010, *MNRAS*, 405, 1047
- Hamann, W.-R., Gräfener, G., Liermann, A., et al. 2019, *A&A*, 625, A57
- Henney, W. J. & Arthur, S. J. 2019, *MNRAS*, 486, 4423
- Jiménez-Hernández, P., Arthur, S. J., Toalá, J. A., et al. 2021, *MNRAS*, 507, 3030
- Jiménez-Hernández, P., Arthur, S. J., & Toalá, J. A. 2020, *MNRAS*, 497, 4128
- Kochanek, C. S. 2011, *ApJ*, 743, 73
- Kharchenko, N. V., Scholz, R.-D., Piskunov, A. E., et al. 2007, *Astronomische Nachrichten*, 328, 889
- Koning N., Steffen W., 2012, *ascl.soft*, *ascl:1204.010*
- Luridiana, V., Morisset, C., & Shaw, R. A. 2015, *A&A*, 573, A42
- Marchenko S. V., Moffat A. F. J., Crowther P. A., 2010, *ApJL*, 724, L90
- Meaburn J., López J. A., Gutiérrez L., Quiróz F., Murillo J. M., Valdéz J., Pedrayez M., 2003, *RMxAA*, 39, 185
- Meyer, D. M.-A., Oskinova, L. M., Pohl, M., et al. 2020, *MNRAS*, 496, 3906
- Moffat, A. F. J., Lamontagne, R., & Seggewiss, W. 1982, *A&A*, 114, 135
- Moffat A. F. J., Isserstedt J., 1980, *A&A*, 85, 201
- Paczynski, B. 1967, *Acta Astron.*, 17, 355
- Podsiadlowski, P., Ivanova, N., Justham, S., et al. 2010, *MNRAS*, 406, 840
- Sévigny, M., St-Louis, N., Drissen, L., et al. 2021, *MNRAS*, 501, 5350
- Schröder, S. L., MacLeod, M., Loeb, A., et al. 2020, *ApJ*, 892, 13
- Sirianni M., Nota A., Pasquali A., Clampin M., 1998, *A&A*, 335, 1029
- Solf, J. & Carsenty, U. 1982, *A&A*, 116, 54
- Steffen, W., Koning, N., Wenger, S., et al. 2011, *IEEE Transactions on Visualization and Computer Graphics*, 17, 454
- Toalá, J. A., Oskinova, L. M., Hamann, W.-R., et al. 2018, *ApJ*, 869, L11
- Vamvatira-Nakou C., Hutsemékers D., Royer P., Waelkens C., Groenewegen M. A. T., Barlow M. J., 2016, *A&A*, 588, A92
- Toalá, J. A. & Arthur, S. J. 2011, *ApJ*, 737, 100
- Tody, D. 1993, *Astronomical Data Analysis Software and Systems II*, 52, 173
- van der Sluis M. V., Lamers H. J. G. L. M., 2003, *A&A*, 398, 181
- Zou, Y., Frank, A., Chen, Z., et al. 2020, *MNRAS*, 497, 2855.
doi:10.1093/mnras/staa2145

This paper has been typeset from a $\text{\TeX}/\text{\LaTeX}$ file prepared by the author.